

Supporting Information

Self-Assembled DNA Nanopores that Span Lipid Bilayers

Jonathan R. Burns¹, Eugen Stulz², Stefan Howorka^{1*}

¹ *Department of Chemistry, Institute of Structural Molecular Biology, University College London, London WC1H 0AJ, England, United Kingdom*

² *School of Chemistry, University of Southampton, Highfield, Southampton SO17 1BJ, United Kingdom*

Table of contents

1. Materials.....	3
2. Methods.....	3
2.1. Design of the DNA nanopore.....	3
2.2. Alkylation of phosphorothioate-DNA	6
2.3. Assembly.....	6
2.4. Size exclusion chromatography	6
2.5. Melting point analysis using UV-vis absorption spectroscopy.....	6
2.6. Dynamic light scattering	7
2.7. Atomic force microscopy.....	7
2.8. Agarose gel electrophoresis	7
2.9. Polyacrylamide gel electrophoresis	7
2.10. Nanopore recordings.....	7
3. Results.....	9
3.1. Chemical modification of PPT-DNA with iodo-ethane.....	9
3.2. Melting point analysis of the DNA-nanobarrel.....	10
3.3. Assessing the structural integrity of DNA-barrels with agarose gel electrophoresis	11
3.4. Examining DNA-barrels with AFM	12
3.5. Nanopore recordings.....	14
3.6. The DNA nanopore is compatible with the widely used honeycomb design of DNA nanoarchitectures	15

1. Materials

Conventional and phosphorothioate-modified DNA oligonucleotides were purchased from Integrated DNA Technologies (Leuven, Belgium) on a 1 μ mole scale with HPLC purification. Diphytanoyl phosphatidylcholine was procured from Avanti Polar Lipids, Alabaster, AL. All other reagents and solvents were purchased from Sigma-Aldrich and used as received unless stated otherwise.

2. Methods

2.1. Design of the DNA nanopore

The DNA barrel with hexagonally arranged DNA-duplex cylinders (Fig. S1) was designed using the cadnano software¹ following the standard honeycomb pattern. The suggested plasmid scaffold strand was replaced by six DNA oligonucleotide scaffold strands because these synthetic nucleic acids can be readily obtained with phosphorothioate groups. The positions of the phosphorothioate (PPT) groups within the scaffold and selected staple strands were determined by inspecting a structural model of the DNA nanopore which had been generated using MacroModel by Schrödinger (Figure S-2). PPT modifications were selected to face the external perimeter of the origami structure within the hydrophobic belt (Figure S2). The sequences of the staple and scaffold strands featuring the marked position of PPT groups are summarized in Table S-1, and Figure S-3 provides the alignment of strands within the DNA barrel.

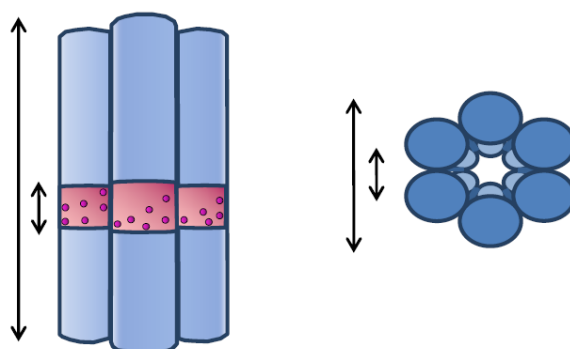


Figure S-1. Structural model of the DNA nanopore in side view (left) and top view (right). The pore is 15 nm high, and the purple hydrophobic belt measures 2.2 nm in height. The outer diameter of the pore is 5.5 nm which compares to an inner channel width of 1.5 nm.

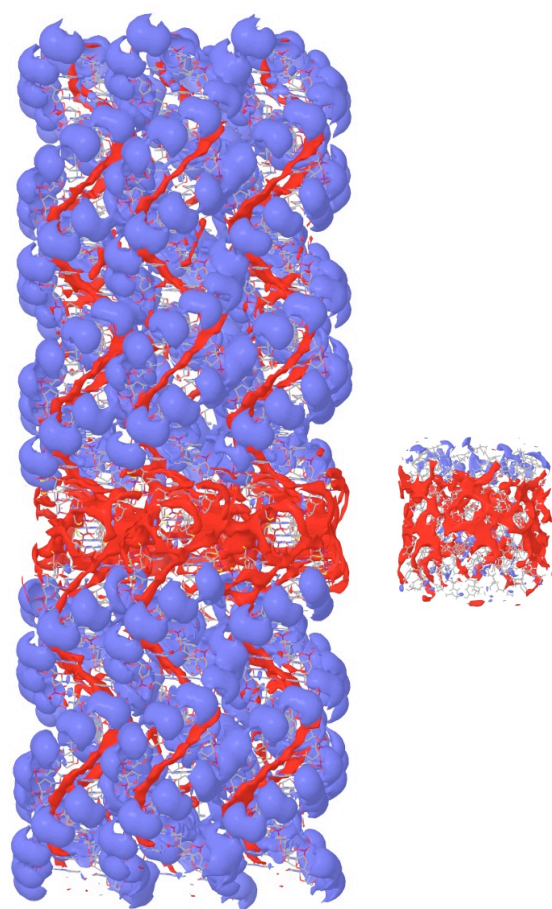


Figure S-2. Structural model of the DNA nanopore (left) illustrating that its hydrophobic belt composed of ethane-PPT groups is comparable in size and hydrophobicity to the lipid bilayer-spanning β -barrel of the α -hemolysin pore (right, PDB-ID 7AHL). The structural models with the calculated hydrophobic (red), hydrophilic (blue) and neutral (transparent) surfaces were generated using MacroModel by Schrödinger.

Table S-1. Sequences of DNA oligonucleotides for assembling the DNA-nanopore

ID	Type ¹	Sequence ²
1	ST	5'-GCGGGGAGCGTATTAGAGTTG-3'
2	ST	5'-TGTTCCAAATAGCCAAGCGGT-3'
3	ST	5'-AGTGAGATGTCGTGACGTGGA-3'
4	ST	5'-ATCGGCATTAAAGACCAGCTGCATTAATTTTTTCTCCTTCAC-3'
5	ST	5'-CAACAGCATCCTGTTTTCCGAA-3'
6	ST	5'-TCCACTAAAATCCCCCAGCAGGCGAAATGATTGCTTTTACC-3'
7	SC	5'-TCCACGTTCTTTAATAGTGGA C*T*C*T*T*G*TTCCAAACTGGAACA-3'
8	SC	5'-GGCTATTCTTTTGAT*T*T*A*T*A*A GGGATTTTGCCGATTTTCGGAA-3'
9	SC	5'-ACAGGATTTTCGCCTGCTGGGG*C*A*A*A*C*CAGCGTGGACCGCTT-3'
10	SC	5'-CAACTCTCTCAGGGC*C*A*G*G*C*GGTGAAGGCAATCAGCTGTTG-3'
11	SC	5'-TCTCACTGGTGAAAAGAAAA C*C*A*C*C*C*TGGCGCCAATACGC-3'
12	SC	5'-TCCCCGCGCGTTGGC*C*G*A*T*T*CATTAAATGCAGCTGGCACGACA-3'
13	ST	5'-CCACGCTCCCTGAGGGGCGCCA*G*G*G*T*G*GG*A*A*T*C*G*GA*C* A*A*G*A*G-3'
14	ST	5'-C*G*C*C*T*G*GG*G*T*T*T*G*CT*T*A*T*A*A*ATCAAAAGGTTTGGACCA ACGC-3'

¹ ST, Staple strand; SC, scaffold strand.

² * indicates a phosphorothioate group between two nucleosides.

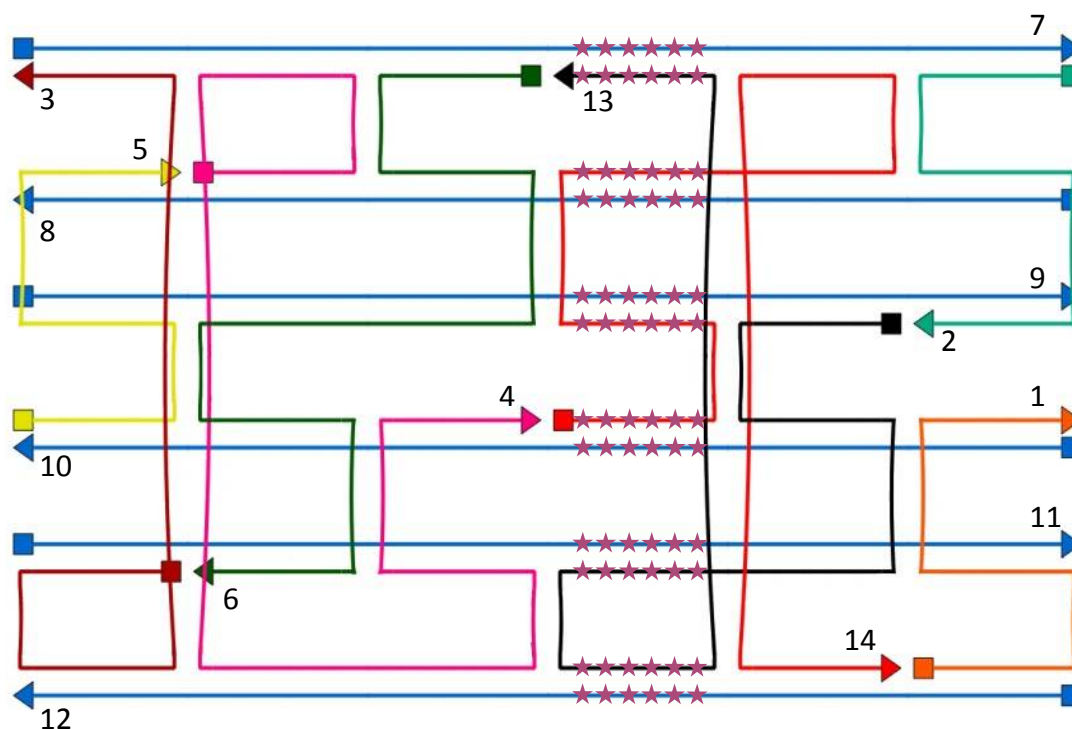


Figure S-3. Map of DNA nanobarrel composed of scaffold strands (DNA oligos 7 to 12) and staple strands (DNA oligos 1-6 and 13 and 14). The stars indicate the phosphorothioate groups.

2.2. Alkylation of phosphorothioate-DNA

Chemical modification of phosphorothioate (PPT)-containing DNA oligonucleotides was conducted by following a modified version of a protocol by Gut and Beck.² For a modification extent of 70%, PPT-carrying DNA oligonucleotides (5 nanomoles each) dissolved in 90% DMF 10% 30 mM Tris-HCl pH 8.0 (250 μ L) were mixed with iodo-ethane (10 equivalents per PPT group) which had been purified by filtration over a silica gel column. The mixture was incubated at 55 °C for 1.5 hours. For a complete modification extent, 20 equivalents were used and the incubation was conducted at 65 °C for 1.5 hours. In both cases, the solvent was removed under reduced pressure, and the resulting dry solid was dissolved in deionized water (50 μ L) to facilitate the removal of excess iodo-ethane via gel permeation using a NAP-25 column (GE Healthcare). Elution of DNA was monitored by absorption at 260 nm via UV-Vis spectroscopy. The DNA fraction was purified by reversed phase HPLC using a Varian ProStar system with a Model 210 solvent delivery module and a Model 320 UV detector. The purification was performed using a Varian C18 column (250 x 4.6 mm, 5 μ m beads, flow rate of 1 mL/min) using the following gradient: at 0 min 98% triethyl ammonium bicarbonate buffer (TEAB) pH 8.0 / 2% acetonitrile (ACN), from 0.1 to 20 min, 70% TEAB/ 30% ACN; from 20.1 to 25 min, 2% TEAB/ 98% ACN; from 25 to 30 min, 98% TEAB/ 2% ACN.

2.3. Assembly

A mixture of equimolar amounts of DNA oligonucleotides (1.5 nM each, dissolved in buffer A: 1.85 M KCl, 50 mM Tris pH 8.0; total volume 500 μ L) was prepared at room temperature, heated at 95 °C for 5 min, and cooled to 16 °C by 0.13 °C per minute in a Varian Cary 300 Bio UV-Vis Spectrophotometer equipped with a Peltier cooling element.

2.4. Size exclusion chromatography

Assembly products were analyzed using an ÄKTA purifier 100/10 fitted with a Superdex 200 10/300 GL column (GE Healthcare). Typically, SEC was performed on a sample containing 5 μ M of DNA origami (100 μ L) dissolved in buffer A using a flow rate of 0.25 mL per minute at 8 °C. Elution was monitored via UV-vis absorption at 260, 280 and 295 nm. SEC-purified samples were used for the ensuing characterization. SEC-purified nanobarrels were optionally concentrated using evaporation of solvent via speed-vac centrifugation and then desalted.

2.5. Melting point analysis using UV-vis absorption spectroscopy

Melting point analysis was performed using a Varian Cary 300 Bio UV-vis Spectrophotometer equipped with a Peltier element and a quartz cuvette with a path length of 1 cm. The samples with a DNA barrel concentration of 0.2 μ M in 1.85 M KCl, 50 mM Tris, pH 8.0 were heated at 0.5 °C to per minute, and absorbance changes at 260 nm were monitored.

2.6. Dynamic light scattering

DLS experiments were conducted on a Zetasizer Nano S from Malvern as described.³ DNA samples were diluted in 1.85 M KCl, 50 mM Tris with a pH of either 8.0 or 5.0 yielding a final barrel concentration of 0.25 μ M.

2.7. Atomic force microscopy

DNA barrels were analyzed by first adsorbing them onto mica following a modified version of published procedure.⁴ Briefly, freshly cleaned mica was incubated with a solution of 3 mM MgCl₂ for 5 min and then repeatedly washed with ddH₂O. The surface was then incubated with a 5-100 nM solution of the DNA-barrel solution which had been cleared of particulate matter by centrifugation at 16,000 rpm for 20 min at 4 °C.

AFM topographical images were acquired in situ at room temperature with a Multimode atomic force microscope with a Nanoscope IV controller (Bruker Santa Barbara, US) and a reflective golden coated (back side) MSNL cantilever. The nominal spring constant of the MSNL cantilever was 0.06N/m and the resonance frequency was 7.3 kHz. Images were analyzed using Nanoscope Analysis software.

2.8. Agarose gel electrophoresis

The assembled DNA barrels were analyzed using 0.8 % agarose gel electrophoresis using standard TBE buffer 45 mM Tris, 45 mM boric acid, 1 mM EDTA, pH 8.3 supplemented with 11 mM MgCl₂. A solution containing 10 picomoles of DNA was mixed with 2 μ L of gel loading dye before loading into the wells. The gel was run at 80 volts for 80 minutes at 8 °C. The bands were visualized by staining in ethidium bromide solution and UV illumination. A 100 base-pair marker was used as reference standard for migration.

2.9. Polyacrylamide gel electrophoresis

DNA phosphorothioate alkylation was monitored using PAGE. A 16 % polyacrylamide gel was used in combination with a 5 % stacking gel. 0.1 nanomole of DNA was mixed with 5 μ L of gel loading dye buffer and 5 μ L of a solution of 6 M urea, followed by heating to 95 °C before loading onto the gel. The gel was run at 160 volts for 1 hour, after which the bands were visualized using ethidium bromide stain. A 50 base-pair marker was used as reference standard for migration.

2.10. Nanopore recordings

Single-channel current recordings were performed by using a planar lipid bilayer apparatus as described.⁵ Briefly, a bilayer of 1,2-diphytanoyl-sn-glycero-3-phosphocholine (Avanti Polar Lipids) was formed on an aperture (120 μ m in diameter) in a Teflon septum (Goodfellow Corporation, Malvern, PA) separating the cis and trans chambers of the apparatus. Each compartment contained 1.0 M KCl, 50 mM Tris-HCl, pH 5.0. It is noted that Tris was retained from the above mentioned

experiments to prepare the nanopore recording electrolyte at pH 5.0 as switching to a different buffer would have introduced another variable. DNA-nanopore was added to the cis compartment at a final concentration 2.5 to 10 nM / mL to achieve insertion of a single channel into the bilayer. Transmembrane currents were recorded at a holding potential of +100 mV (with the cis side grounded) unless stated otherwise by using a patch-clamp amplifier (Axopatch 200B, Axon Instruments, Union City, CA) connected to Digidata 1200 A/D converter (Axon Instruments) at a low-pass filtering frequency of 10 and a sampling frequency of 50 kHz.⁶ Current traces were optionally acquired with the Orbit 16 system from Nanion connected either to an EPC 10 Plus Heka single channel or a Tecella Triton 16 channel amplifier. Currents were low-pass filtered at 3 kHz and sampled at 10 kHz.

3. Results

3.1. Chemical modification of PPT-DNA with iodo-ethane

Chemical treatment with ethyl-iodide of DNA strand SC7 carrying six PPT groups resulted in a peak shift from 12.7 min to 16.3 minutes (Figure S-4A) implying complete modification. A complete extent of modification was also observed when DNA strand ST14 with 18 PPT groups was analyzed using PAGE (Figure S-4B). To confirm the chemical nature of the modification via mass spectrometry, we analyzed DNA oligonucleotide C carrying a single PPT-group. The sequence of the 31-mer is 5'-CGATGA AGATGCGTCCT*TCGTCACGAGTCCT-3' with * marking the position of the PPT group. Mass spectrometric analysis confirmed that the mass of ethane-modified PTT-oligonucleotide is in line with expectations (Figure S-5).

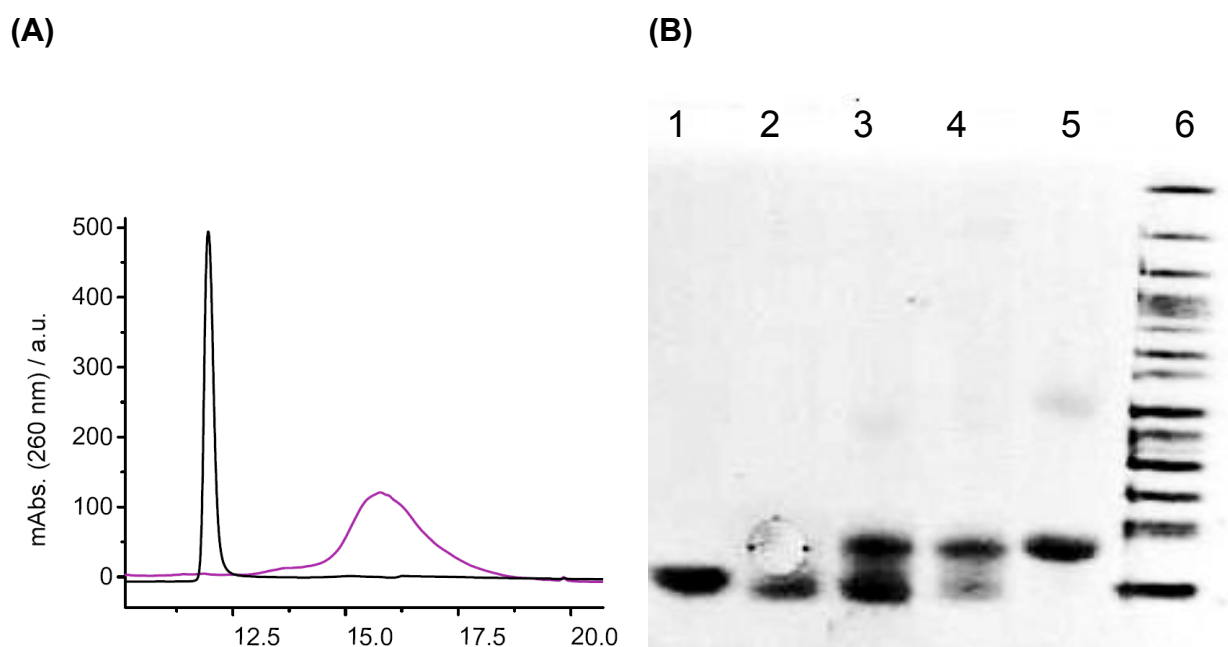


Figure S-4. Tracking the chemical modification of PPT-containing DNA strands with ethyl-iodide. (A) HPLC trace of DNA oligonucleotide SC7 carrying six PPT groups, before (red line) and after (black line) incubation with iodoethane. (B) Electropherogram for the PAGE analysis of strand ST14 with 18 PPT groups incubated with 10 equivalents of iodo-ethane (lanes 1 to 4) and 20 equivalents (lane 5). Lane 1, after 0 min and no heating; lane 2, after 10 min of heating at 55 °C; lane 3, after 20 min of heating at 55 °C; lane 4, after 30 min of heating at 55 °C; lane 5, 90 min at 65 °C; lane 6, DNA ladder with 50 bp steps.

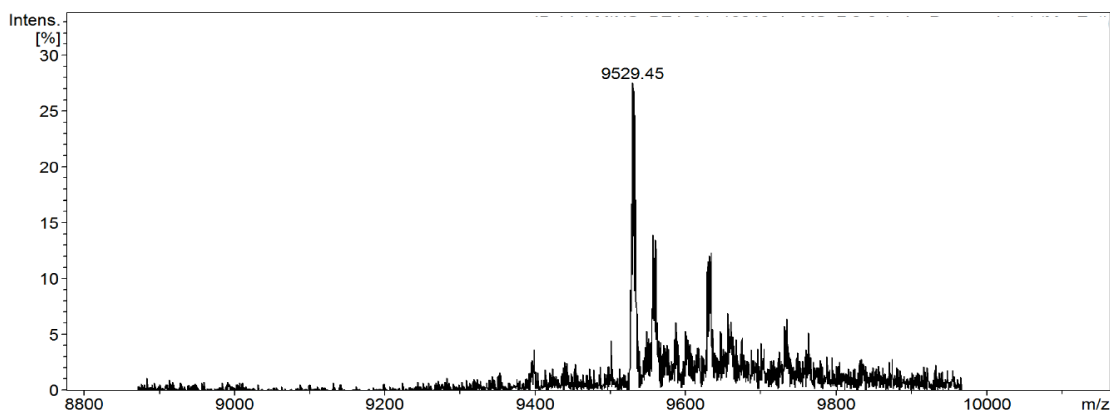


Figure S-5. ESI Micro-ToF analysis of the iodo-ethane modified control strand C carrying a single PPT group. Calculated MS, 9531.20; found MS, = 9529.45.

3.2. Melting point analysis of the DNA-nanobarrel

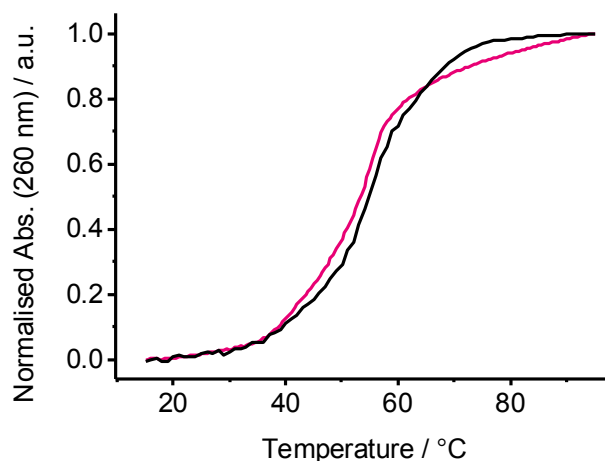


Figure S-6. UV-melting profile of the DNA nanopore. 0.2 μ M DNA barrels 1.85 M KCl, 50 mM Tris pH 8. were heated at 0.5 $^{\circ}$ C per minute. The graph shows the profiles of DNA-barrels with PPT groups (black line) and ethane-PPT groups (red line).

UV-melting analysis of DNA-barrels with PPT groups yielded a melting temperature, T_m , of 53.2 ± 1.7 $^{\circ}$ C ($n = 5$; n , number of independent experiments). By comparison, the value of T_m for the barrel with 70% alkylation of the PPT groups was 51.8 ± 1.5 $^{\circ}$ C, which is within the error of measurement of the non-modified DNA barrel. The match of the two melting temperatures indicates that the chemical modification did not change the overall stability of the DNA barrels. This observation is at first sight surprising as T_m could have theoretically increased upon capping of the negatively charged phosphorothioates causing a removal of the inter-strand electrostatic repulsion.⁷ But a more comprehensive view would also consider a compensatory destabilization due to the randomized,

alkylation-induced locking of phosphorothioates into either the R_P or S_P isomer conformation and its effect on duplex structure.⁷ In support of this view, 100 % alkylation-barrels had a lowered T_m of 46.4 °C (data not shown).

The experimental melting profiles of DNA nanopores are also instructive as the presence of a single as opposed to multiple melting transitions implies a high degree of cooperativity in the unfolding and folding process. The DNA nanobarrel is composed of several duplex segments of different length which –when assembled and dissociated independently- would give rise to multiple melting transitions. By contrast, a single transition is strong evidence for the simultaneous hybridization of all strands. Indeed, the range of melting temperature for the individual component strands is large as exemplified for scaffold strand 7 (82.5 °C), staple strand 5 (71.8 °C), and a typical 7-mer duplex (15.6 °C). These calculated values illustrate the T_m range but cannot be directly compared to the experimental data for the nanopore because the available software tools do not provide predictions for DNA strands with phosphorothioates.

3.3. Assessing the structural integrity of DNA-barrels with agarose gel electrophoresis

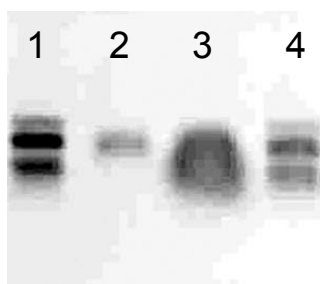


Figure S-7. Electropherogramm of DNA barrels in a 0.8 % agarose gel. Lane 1, 100 bp marker with 500 and 1000 bp of increased intensity; lane 2, PPT-DNA barrel; lane 3, ethane-modified DNA barrel; lane 4, 100 bp marker.

The PPT-DNA barrel migrates as a single sharp band (Figure S-7, lane 2) at a height of 1000 bp. The migration as a sharp band implies that the nanobarrel is stable under the gel electrophoretic conditions of low ionic strength of 45 mM Tris and 45 mM boric acid. By comparison, the ethane-modified version migrates faster and as a broad band (Figure S-7, lane 3) suggesting that this barrel unfolds. The increased electrophoretic mobility of an unfolded barrel was established by denaturing the sample prior to running a gel (data not shown). The destabilization of the ethane-modified PPT-barrel likely results from the low ionic strength of the electrophoresis buffer as observed for other DNA nanostructures.⁸ The barrels were stable in higher ionic strength buffer used in size exclusion chromatography (Figure 3, main paper) and dynamic light scattering (Figure 4A, main paper).

3.4. Examining DNA-barrels with AFM

Barrels were analyzed with AFM at a final concentration of 5 nM and 100 nM. At 5 nM, individual nanobarrels and tubes of non-covalent end-to-end stacked nanobarrels were observed (Figure S-8). By comparison, the high concentration led to complete coverage with DNA barrels which were mostly assembled into arrays of the end-to-end-stacked tubes (Figure S-9). Similar π -stacking-induced assembly has been observed for other DNA nanostructures.⁹

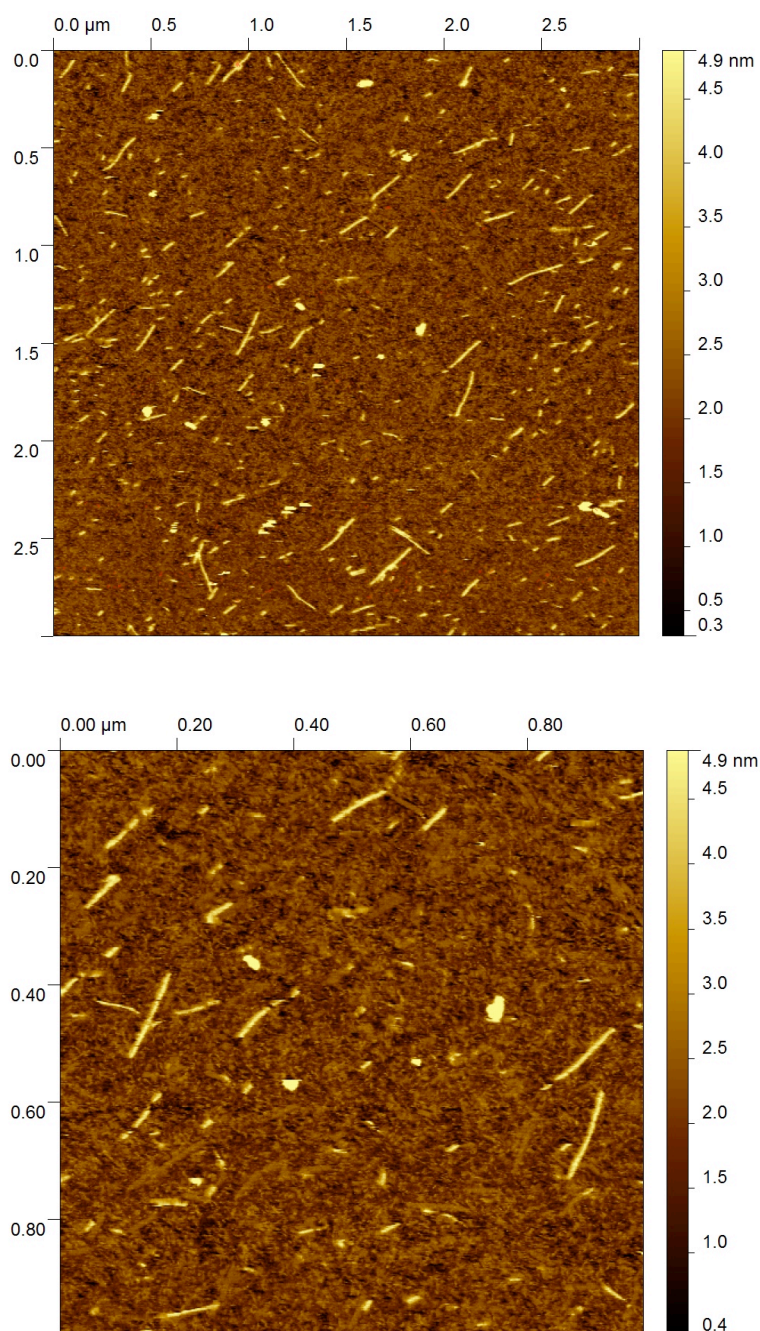


Figure S-8. AFM micrograph of DNA barrel adsorbed at a final concentration 5 nM in 0.1 M KCl, 3 mM MgCl₂, 0.01 M Tris pH 8.0. The features with the shortest length were subjected to analysis.

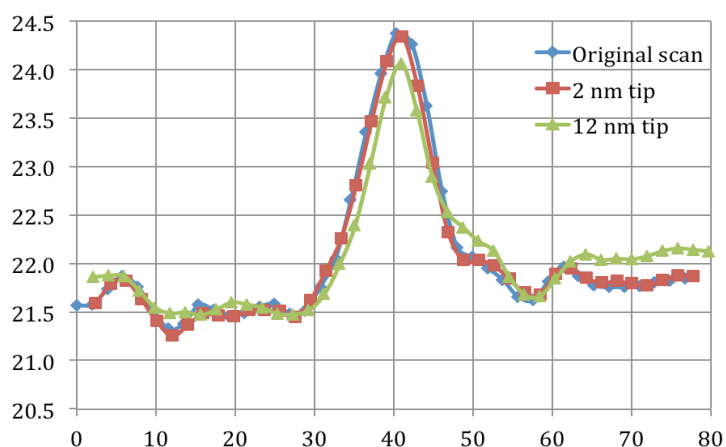


Figure S-9. AFM height profiles of an isolated DNA nanobarrel (blue trace) and surface reconstructed data of a DNA nanobarrel for tips of 2 nm (red) and 12 nm (green) tip radii respectively. The surface reconstruction was calculated as described.¹⁰

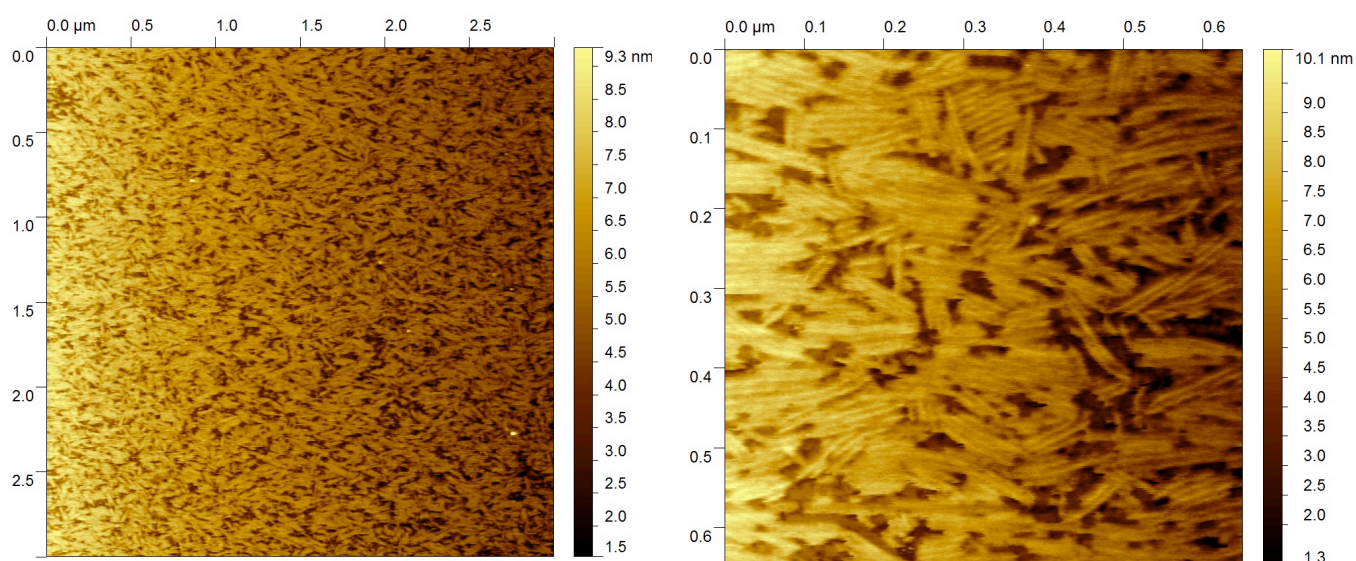


Figure S-10. AFM micrograph of DNA barrel adsorbed at a final concentration 100 nM in 0.1 M KCl, 3 mM MgCl₂, 0.01 M Tris pH 8.0.

3.5. Nanopore recordings

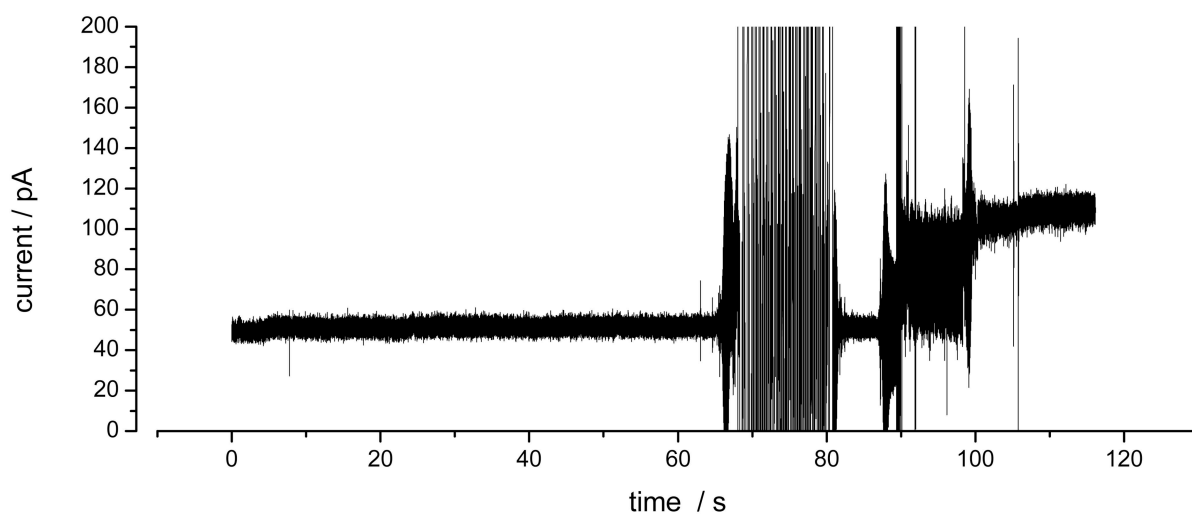


Figure S-11. Current trace showing the insertion of a second DNA nanopore channel at 100 seconds after opening the Faraday cage and adding nanopore solution at around 70 s, and stirring the electrolyte solution from 90 to 100 s.

3.6. The DNA nanopore is compatible with the widely used honeycomb design of DNA nanoarchitectures

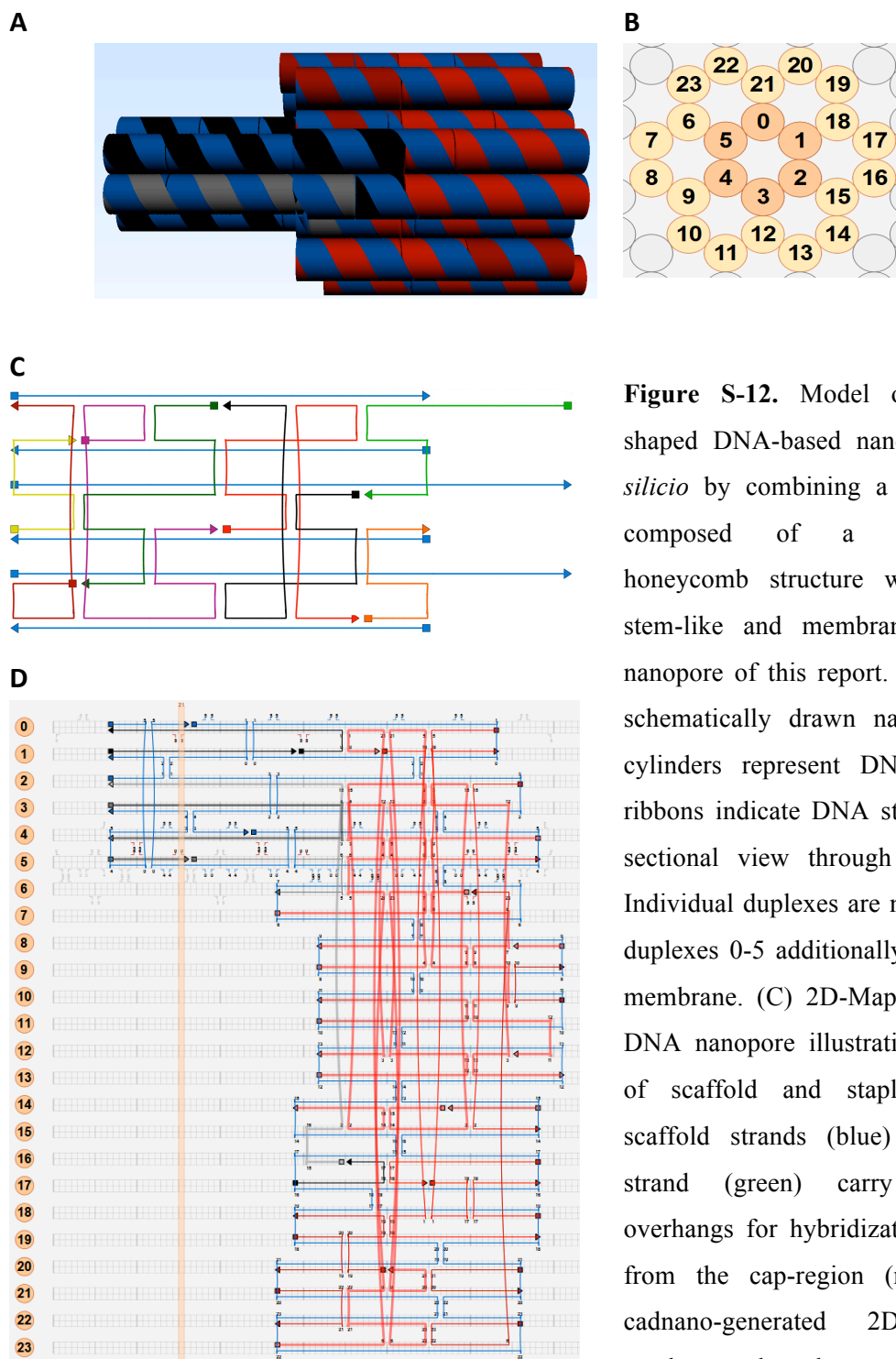


Figure S-12. Model of a mushroom-shaped DNA-based nanochannel built *in silico* by combining a large cap region composed of a cadnano-designed honeycomb structure with the smaller, stem-like and membrane-passing DNA-nanopore of this report. (A) Side view of schematically drawn nanochannel where cylinders represent DNA duplexes and ribbons indicate DNA strands. (B) Cross-sectional view through the cap region. Individual duplexes are numbered. Central duplexes 0-5 additionally span the bilayer membrane. (C) 2D-Map of the stem-like DNA nanopore illustrating the alignment of scaffold and staple strands. Two scaffold strands (blue) and one staple strand (green) carry single-stranded overhangs for hybridization to extensions from the cap-region (not shown). (D) cadnano-generated 2D-map of the mushroom-shaped nanochannel featuring the stem section (duplexes 0-5) and the cap (duplexes 0 – 23).

References:

1. Douglas, S. M.; Marblestone, A. H.; Teerapittayanon, S.; Vazquez, A.; Church, G. M.; Shih, W. M. *Nucleic Acids Res.* **2009**, *37*, (15), 5001-5006.
2. Gut, I. G.; Beck, S. *Nucleic Acids Res.* **1995**, *23*, (8), 1367-1373.
3. Clifton, L. A.; Sanders, M. R.; Castelletto, V.; Rogers, S. E.; Heenan, R. K.; Neylon, C.; Frazier, R. A.; Green, R. J. *Phys. Chem. Chem. Phys.* **2011**, *13*, (19), 8881-8888.
4. Mitchell, N.; Ebner, A.; Hinterdorfer, P.; Tampe, R.; Howorka, S. *Small* **2010**, *6*, (16), 1732–1735.
5. Braha, O.; Walker, B.; Cheley, S.; Kasianowicz, J. J.; Song, L.; Gouaux, J. E.; Bayley, H. *Chem. Biol.* **1997**, *4*, (7), 497-505.
6. Movileanu, L.; Howorka, S.; Braha, O.; Bayley, H. *Nat. Biotechnol.* **2000**, *18*, (10), 1091-1095.
7. Vangenderen, M. H. P.; Koole, L. H.; Aagaard, O. M.; Vanlare, C. E. J.; Buck, H. M. *Biopolymers* **1987**, *26*, (9), 1447-1461.
8. O'Neill, P.; Rothmund, P. W. K.; Kumar, A.; Fygenson, D. K. *Nano Lett.* **2006**, *6*, (7), 1379-1383.
9. Rothmund, P. W. *Nature* **2006**, *440*, (7082), 297-302.
10. Klapetek, P.; Ohlídal, I. *Ultramicroscopy* **2003**, *94*, 19-29.